JBC RESEARCH ARTICLE

Hepatocyte estrogen sulfotransferase inhibition protects female mice from concanavalin A–induced T cell–mediated hepatitis independent of estrogens

Received for publication, October 24, 2022, and in revised form, February 7, 2023 Published, Papers in Press, February 15, 2023,
https://doi.org/10.1016/j.jbc.2023.103026

Jingyuan Wang[1], Ziteng Zhang[1], Jibin Guan[1], Hung-Chun Tung[1], Jiaxuan Xie[1], Haozhe Huang[1], Yuang Chen[1], Meishu Xu[1], Songrong Ren[1], Song Li[1], Min Zhang[1], Da Yang[1], and Wen Xie[1,2,*]

From the [1]Center for Pharmacogenetics and Department of Pharmaceutical Sciences, and [2]Department of Pharmacology & Chemical Biology, University of Pittsburgh, Pittsburgh, Pennsylvania, USA

Reviewed by members of the JBC Editorial Board. Edited by Ronald Wek

Autoimmune hepatitis (AIH) is a typical T cell–mediated chronic liver disease with a higher incidence in females. However, the molecular mechanism for the female predisposition is poorly understood. Estrogen sulfotransferase (Est) is a conjugating enzyme best known for its function in sulfonating and deactivating estrogens. The goal of this study is to investigate whether and how Est plays a role in the higher incidence of AIH in females. Concanavalin A (ConA) was used to induce T cell–mediated hepatitis in female mice. We first showed that Est was highly induced in the liver of ConA-treated mice. Systemic or hepatocyte-specific ablation of Est, or pharmacological inhibition of Est, protected female mice from ConA-induced hepatitis regardless of ovariectomy, suggesting the effect of Est inhibition was estrogen independent. In contrast, we found that hepatocyte-specific transgenic reconstitution of Est in the whole-body Est knockout (EstKO) mice abolished the protective phenotype. Upon the ConA challenge, EstKO mice exhibited a more robust inflammatory response with elevated production of proinflammatory cytokines and changed liver infiltration of immune cells. Mechanistically, we determined that ablation of Est led to the hepatic induction of lipocalin 2 (Lcn2), whereas ablation of Lcn2 abolished the protective phenotype of EstKO females. Our findings demonstrate that hepatocyte Est is required for the sensitivity of female mice to ConA-induced and T cell–mediated hepatitis in an estrogen-independent manner. Est ablation may have protected female mice from ConA-induced hepatitis by upregulating Lcn2. Pharmacological inhibition of Est might be a potential strategy for the treatment of AIH.

Autoimmune hepatitis (AIH) is a T cell–mediated chronic liver disease. Like many other forms of autoimmune diseases, AIH shows a female preponderance and can affect both children and adults (1, 2). Patients with AIH usually present with jaundice, fatigue, elevated serum transaminase and IgG levels, and histological interface hepatitis, which are signs of acute hepatitis (3). In some cases, AIH can present as fulminant hepatic failure due to the massive destruction of hepatocytes. If the autoimmune process remains uncontrolled, hepatocytes will be continuously affected and damaged, which can lead to a rapid loss of liver function, fibrosis, cirrhosis, or even hepatocellular carcinoma. Patients with AIH who develop fulminant hepatic failure that is unresponsive to traditional corticosteroid treatment may need liver transplantation, but recurrent AIH can occur after the transplantation (2). Concanavalin A (ConA) is a lectin (carbohydrate-binding protein) extracted from jack beans. ConA-induced hepatitis is a typical and well-established mouse model of AIH (4, 5), because it can faithfully recapitulate the T cell–mediated liver damage observed in patients with AIH (2, 6). Moreover, the female mice were more susceptible to ConA-induced hepatitis than their male counterparts (7), consistent with the female predisposition of AIH in patients.

Estrogen sulfotransferase (EST, or SULT1E1) is a member of the cytosolic sulfotransferase family. EST is best known for its activity in sulfonating and deactivating estrogens because the sulfonated estrogens cannot bind to and activate the estrogen receptor. In both humans and mice, EST is expressed in many tissues, including the liver. The basal expression of Est in the mouse liver was low, but its expression was highly inducible in response to several systemic or organ-specific diseases that involve inflammation, such as sepsis, liver ischemia-reperfusion, obesity and type two diabetes, acute kidney injury, and hemorrhagic shock-induced acute lung injury (8–13). AIH is also an inflammatory liver disease, but the role of EST in AIH and the female predisposition of AIH has not been reported.

Lipocalin-2 (Lcn2), also known as neutrophil gelatinase associated lipocalin in humans, is a member of the lipocalin family. Lcn2 has been reported to have diverse functions, including in innate immunity. Lcn2 can inhibit bacterial growth by sequestering iron and preventing its use by bacteria (14). The hepatic expression of Lcn2 is highly inducible by liver tissue damages, such as those induced by CCl_4, lipopolysaccharide, ConA, and bile duct ligation (15). In these disease models, $Lcn2^{-/-}$ mice exhibited more severe liver

* For correspondence: Wen Xie, wex6@pitt.edu.

damage with heightened inflammatory responses, which suggested a protective effect of Lcn2 in the liver.

In this study, we unveiled the hepatocyte Est as the long-elusive determinant of female sensitivity to T cell–mediated hepatitis independent of estrogens. Genetic ablation or pharmacological inhibition of Est protected female mice from ConA-induced hepatitis. Our results suggest that Est may serve as a therapeutic target for the management of AIH and other T cell–mediated hepatitis.

Results

The hepatic expression of Est is highly induced in the ConA model of hepatitis

To determine whether Est plays a role in T cell–mediated hepatitis, WT C57BL/6j female mice were subjected to tail vein injections of 10 mg/kg ConA to induce T cell–mediated hepatitis before being measured for the hepatic expression of Est. As expected, treatment with ConA was effective to induce hepatitis and liver injury, as evidenced by dramatically increased serum levels of alanine aminotransferase (ALT) and aspartate aminotransferase (AST) (Fig. 1*A*), as well as histological liver necrosis (Fig. 1, *B* and *C*) at 24 h after the ConA injection. Liver necrosis in the ConA model was mainly developed in zone 2, consistent with a previous report (16). When the expression of Est was analyzed, we found the mRNA (Fig. 1*D*) and protein (Fig. 1*E*) expressions of Est were highly induced in the livers of ConA-treated mice, as shown by real-time PCR and immunohistochemistry, respectively. The histological analysis suggested that the induction of Est by ConA occurred generally in the nonnecrotic area without an obvious zonation pattern. The induction of Est appeared to be liver specific, as the basal expression of Est in the white adipose tissues was barely detectable (Cq value 35.6) and the adipose expression of Est remained negligible upon ConA treatment (Cq value 32.1) (Fig. 1*D*). The liver-specific induction of Est by ConA suggested the potential role of this enzyme in T cell–mediated hepatitis.

Systemic genetic ablation or pharmacological inhibition of Est protects female mice from ConA-induced hepatitis

We then used genetic and pharmacological loss-of-function models to determine whether the induction of Est in ConA-induced hepatitis was functionally relevant. In the genetic model, the whole-body Est knockout (EstKO) female mice were subjected to ConA-induced hepatitis. Compared with WT female mice, EstKO females showed a protection from ConA-induced hepatitis, which was evidenced by their lower levels of serum ALT and AST (Fig. 2*A*) and decreased liver

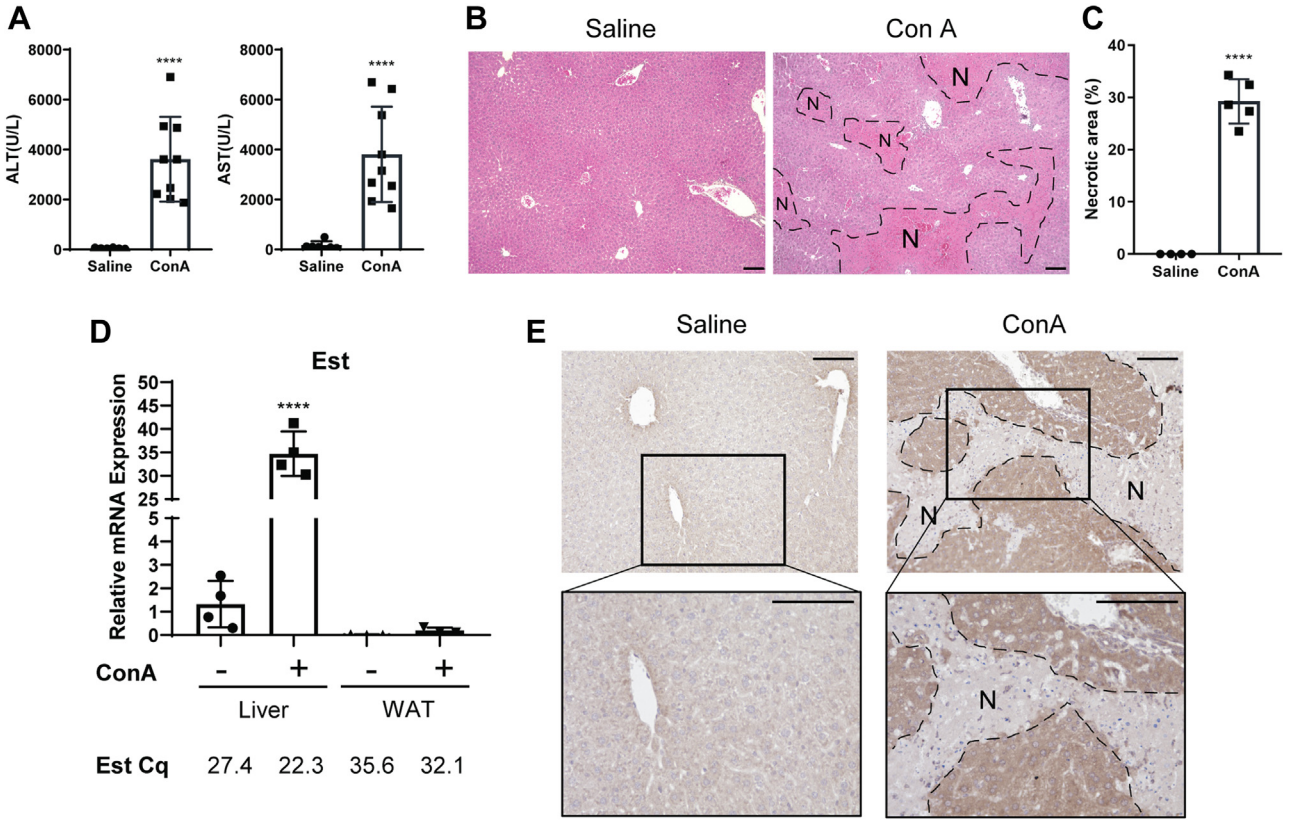

Figure 1. The hepatic expression of Est is highly induced in the ConA model of hepatitis. Eight-week-old female WT mice were treated with saline or 10 mg/kg ConA by tail vein injections, and the tissues and serum were collected 24 h after ConA administration. *A*, serum levels of ALT and AST. *B*, liver histology by H&E staining. *C*, quantification of necrotic area in liver histology. *D*, mRNA expression of Est in liver and white adipose tissues (WAT) measured by quantitative PCR with the Cq values labeled. *E*, immunohistochemical staining of Est in liver sections. The *bottom panels* represent enlarged areas boxed in the *top panels*. *Dashed lines* and "*N*" indicate necrosis. The scale bars represent 100 μm. n = 6 to 9 per group as shown in plots. Data are presented as mean ± SD; ****$p < 0.0001$. ALT, alanine aminotransferase; AST, aspartate aminotransferase. .

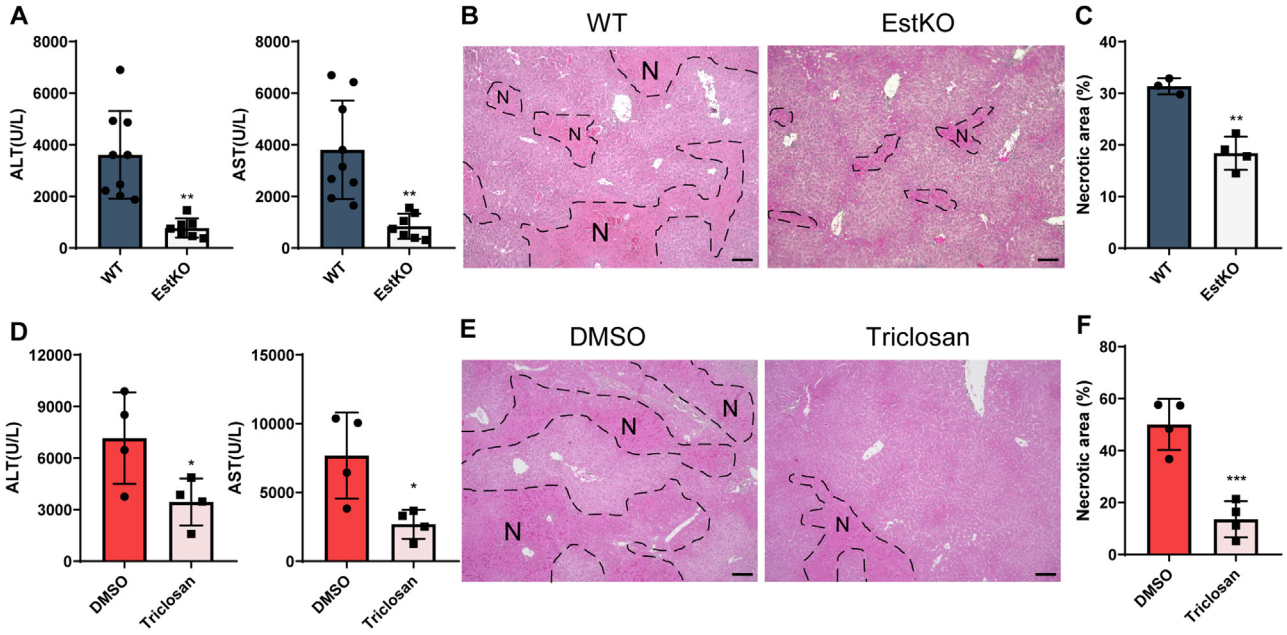

Figure 2. Systemic genetic ablation or pharmacological inhibition of Est protects mice from ConA-induced hepatitis. *A–C*, eight-week-old EstKO female mice were treated with 10 mg/kg ConA by tail vein injections, and the tissues and serum were collected 24 h after ConA administration (n = 7–9 per group as shown in plots). *D–F*, eight-week-old WT female mice were pretreated with 20 mg/kg Triclosan or its solvent DMSO by s.c. injections for 3 days, and ConA (10 mg/kg) was injected on the third day (n = 4 per group). Tissues and serum were collected 24 h after ConA administration. Liver injury was evaluated by the serum levels of ALT and AST (*A* and *D*), liver histology by H&E staining (*B* and *E*) (the representative image of ConA-treated WT mice in *B* is reused from Fig. 1*B* since they are the same group of mice), and quantifications of necrotic area in liver histology (*C* and *F*). *Dashed lines* and "*N*" indicate necrosis. The scale bars represent 100 μm. Data are presented as mean ± SD; $*p < 0.05$, $**p < 0.01$, $***p < 0.001$. ALT, alanine aminotransferase; AST, aspartate aminotransferase; DMSO, dimethyl sulfoxide.

necrosis (Fig. 2, *B* and *C*). In the pharmacological model, treatment of WT female mice with the EST inhibitor Triclosan (17) led to a decreased sensitivity to ConA-induced hepatitis, as supported by their lower serum ALT and AST levels (Fig. 2*D*) and decreased liver necrosis (Fig. 2, *E* and *F*). In both EstKO mice and Triclosan-treated mice, the necrosis was mainly developed in zone 2 as in WT mice, but with smaller area and incidence. These results indicated that inhibition of Est protected female mice from T cell–mediated hepatitis.

The ConA-induced immune response is more robust but less toxic in female EstKO mice

To understand the mechanism for the hepatoprotective effect of Est ablation and knowing that the liver injury in the ConA model of hepatitis is mainly caused by cytokines and cytotoxic immune cells (2, 6), we went on to profile the expression of inflammatory cytokines and immune responses upon the ConA challenge. Surprisingly, the mRNA expression of proinflammatory cytokines Tnfα, Ifnγ, and Il2 was significantly increased in the liver of ConA-treated female EstKO mice, while the mRNA expression of several other cytokines were slightly decreased (Il4 and Il10) or had little change (Il1b and Il17) (Fig. 3*A*). The serum levels of TNFα and IFNγ, two key cytokines in the ConA model, were also elevated in the female EstKO mice at both the early (6 h) and late (24 h) time points after the ConA injections (Fig. 3*B*).

It has been reported that, upon binding to and activating its receptor, TNFα can either induce the apoptotic pathways or activate the prosurvival nuclear factor-kappa B (NF-κB) and mitogen-activated protein kinase (MAPK) signaling pathways, which was facilitated by the prosurvival proteins cellular inhibitors of apoptosis 1 and 2 (c-IAP1 and c-IAP2) (18). Considering the hepatoprotective phenotype of EstKO mice, we speculated that the induction of proinflammatory cytokines in ConA-treated EstKO mice may have triggered the prosurvival responses, leading to an overall protective phenotype. Indeed, the expressions of both c-IAP1 and c-IAP2 were elevated in the livers of EstKO mice (Fig. 3*C*), which were accompanied by the suppression of apoptosis as shown by the terminal deoxynucleotidyl transferase dUTP nick end labeling (TUNEL) assay (Fig. 3*D*), as well as the downregulation of apoptosis marker gene Bax as shown by Western blotting (Fig. 3*E*) and its quantification (Fig. 3*F*).

It is known that, upon the ConA challenge, a large number of mononuclear cells (MNCs) will infiltrate into the liver to facilitate the immune responses (4, 6). We therefore profiled the hepatic infiltration of MNCs by flowcytometry. Consistent with the increase of proinflammatory cytokines that are produced upon T helper cell activation, there were more $CD4^+$ T cells among the hepatic MNCs in EstKO mice 6 h after the ConA injection (Fig. 3, *G* and *H*). Further analysis showed that the percentage of regulatory T cell ($CD4^+Foxp3^+$) was significantly higher, whereas the percentage of cytotoxic $CD8^+$ T cell was decreased (Fig. 3, *G* and *H*) in ConA-treated EstKO mice. Knowing the protective role of Treg and cytotoxic role of CD8+ T cell in the ConA model (6), we reasoned that the profile of MNC infiltration in the liver may have contributed to the protective phenotype of EstKO mice.

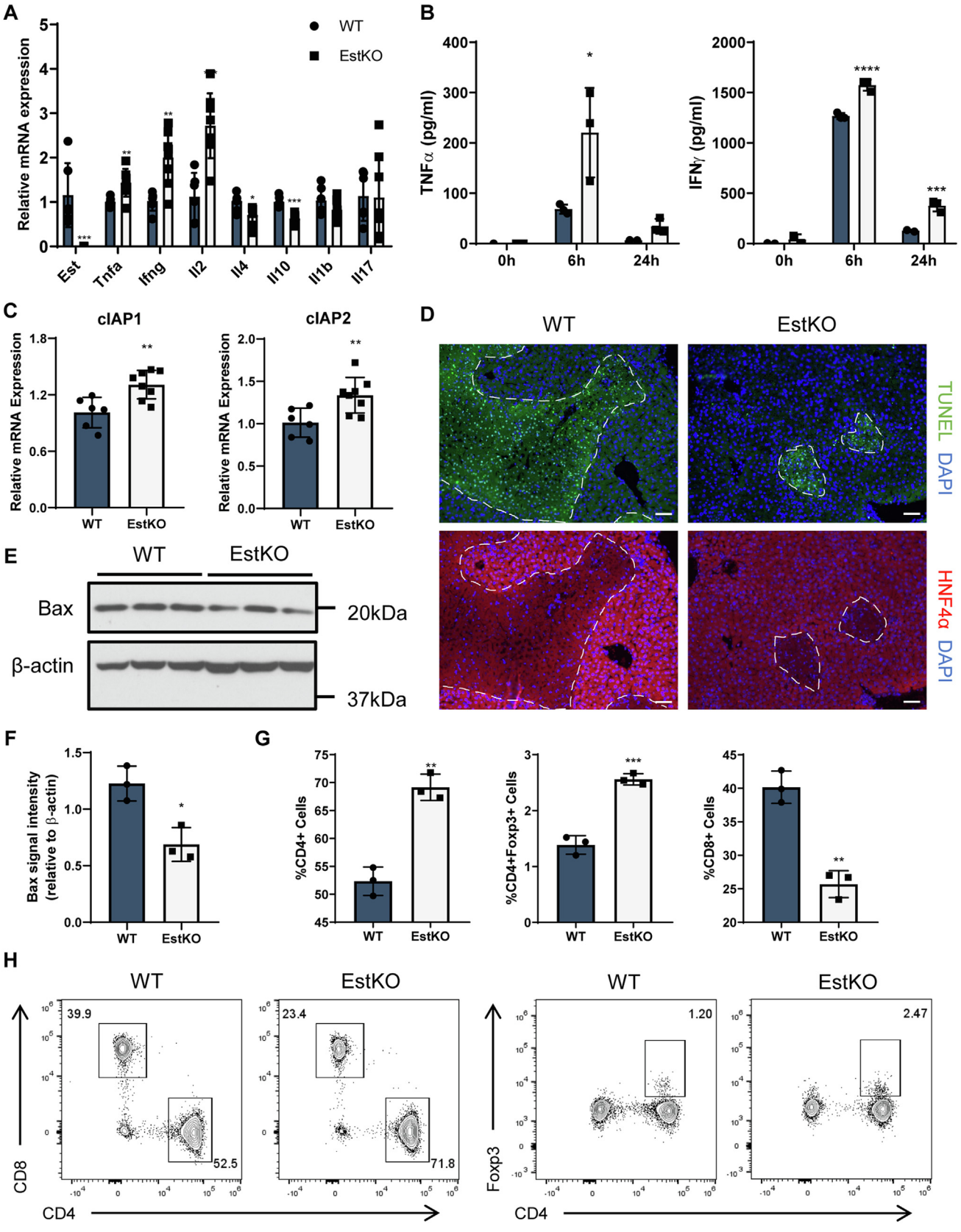

Figure 3. The ConA-induced immune response is more robust but less toxic in female EstKO mice. Eight-week-old WT and EstKO female mice were treated with 10 mg/kg ConA by tail vein injections, and the tissues and serum were collected at 24 h or indicated timepoints after ConA administration. *A*, gene expression of Est and inflammatory cytokines in the liver tissues measured by quantitative PCR. n = 6 to 8 per group as shown in plots. *B*, serum level of TNFα and IFNγ at 6 h and 24 h after the ConA injection measured by ELISA. n = 3 per group. *C*, mRNA expression of cellular inhibitors of apoptosis cIAP1 and cIAP2 in the liver tissue measured by quantitative PCR. n = 6 to 8 per group as shown in plots. *D*, immunofluorescence staining of HNF4α and TUNEL

The attenuation of ConA-induced hepatitis in female EstKO mice is independent of estrogens

Est is best known to sulfonate and deactivate estrogens. We then investigated whether the protection from ConA-induced liver injury in female EstKO mice was estrogen dependent. In this experiment, the endogenous estrogens were depleted by ovariectomy when mice were 4 weeks old, and the mice were challenged with ConA 4 weeks after the ovariectomy surgery as outlined in Figure 4*A*. Ovariectomy alone had little effect on the animal's sensitivity to ConA, as indicated by largely unchanged serum ALT and AST levels (Fig. 4*B*) and liver necrosis (Fig. 4, *C* and *D*). More interestingly, ovariectomized EstKO mice remained protected from ConA-induced liver injury compared with their WT counterparts, as shown by their decreased serum levels of ALT and AST (Fig. 4*B*), liver necrosis (Fig. 4, *C* and *D*), and apoptosis (Fig. 4*E*). These results demonstrated that the protective phenotype observed in ConA-treated EstKO mice was estrogen independent.

Hepatocyte-specific reconstitution of Est abolishes the ConA protective phenotype of EstKO mice

To determine the cellular source of Est that might have contributed to the phenotype, we isolated primary hepatocytes and hepatic nonparenchymal cells (NPCs) from the livers of mice with or without the ConA treatment. Without the ConA treatment, the level of Est was higher in hepatocytes than in NPCs. Upon the ConA challenge, Est was induced in both hepatocytes and NPCs, but the induction was far more dramatic in the hepatocytes (Fig. 5*A*), leading to a markedly higher level of Est expression in hepatocytes than in NPCs (Fig. 5*A*). These results led to our hypothesis that hepatocytes are likely the major source of Est in the liver, especially upon the ConA challenge.

To experimentally define the role of hepatocyte Est in ConA-induced AIH, we reconstituted the expression of Est in the hepatocytes of EstKO mice by breeding the hepatocyte-specific Lap-EST (LE) transgene into the EstKO background, and the resultant mice were termed KOLE mice as outlined in Figure 5*B*. The Lap-EST transgene expresses the human EST gene under the control of the hepatocyte-specific rat liver-enriched activator protein (Lap) gene promoter (12). The reconstitution of EST in the liver of KOLE mice was verified by real-time PCR (Fig. 5*C*). The hepatocyte-specific overexpression of EST was also verified by both Western blotting (Fig. 5*D*) and real-time PCR (Fig. 5*E*). In contrast to the protection observed in the EstKO mice, the KOLE mice developed liver injury comparable with the WT mice, as shown by the serum levels of ALT and AST (Fig. 5*F*) and liver necrosis (Fig. 5, *G* and *H*). In addition to their resensitized liver injury, KOLE mice also had their expression proinflammatory cytokines Tnfα, Ifnγ, and Il2 largely normalized to the levels of WT mice, with the exception of Il4 and Il10 (Fig. 5*I*). The expression of Il4 and Il10 remained suppressed in KOLE mice (Fig. 5*I*). Il4 and Il10 are mainly produced by Th2 cells while Tnfα and Il2 are from Th1 cells. These results suggested that the manipulation of hepatic Est may have differential effects on Th1 and Th2 cells. Moreover, the induction of prosurvival protein genes c-IAP1 and c-IAP2 was also abolished in the KOLE mice (Fig. 5*J*). The increased liver infiltration of $CD4^+$ and Treg percentage and decreased infiltration of $CD8^+$ cells observed in EstKO mice were also largely normalized to the WT levels in KOLE mice (Figs. 5*K* and S2). These results suggested that it was the loss of Est in the hepatocytes that protected the EstKO mice from ConA-induced AIH.

Hepatocyte-specific ablation of Est protects mice from ConA-induced hepatitis independent of estrogens

To determine whether ablation of Est in hepatocytes was sufficient to protect female mice from ConA-induced hepatitis, we generated the $Est^{fl/fl}$ mice by floxing the exons 3 and 4 of the mouse Est gene, along with the insertion of an inverted tdTomato reporter gene, as outlined in Figure 6*A*. The Cre-mediated inversion and consequent inactivation of exons 3 and 4 were initiated by infecting the $Est^{fl/fl}$ mice with the hepatocyte-specific adeno-associated virus vector serotype 8 (AAV8)-thyroxine-binding globulin (TBG)-iCre, and these mice were termed $Est^{\Delta HC}$ mice. Meanwhile, upon the AAV8-TBG-iCre infection, tdTomato was brought into the forward orientation and expressed specifically in the hepatocytes, which was confirmed by the fluorescent signals of tdTOMATO (Fig. 6*B*). The effective downregulation of Est in the liver (Fig. 6*C*) and primary hepatocytes (Fig. 6*D*) of $Est^{\Delta HC}$ mice, compared with AAV8-TBG-eGFP-infected $Est^{fl/fl}$ mice, was verified by real-time PCR. Upon the ConA challenge, the $Est^{\Delta HC}$ mice exhibited a protective effect against ConA-induced AIH compared with the $Est^{fl/fl}$ mice, including lower serum levels of ALT and AST (Fig. 6*E*), as well as decreased liver necrosis (Fig. 6, *F* and *G*). We further verified the estrogen independency of the protective phenotype in these conditional knockout mice by ovariectomy. The ovariectomized $Est^{\Delta HC}$ mice remained protected from ConA-induced AIH based on the serum levels of ALT and AST (Fig. 6*H*) and liver necrosis (Fig. 6, *I* and *J*). These results demonstrated that loss of Est in hepatocytes was sufficient to protect female mice from ConA-induced hepatitis independent of estrogens.

To determine whether the protective effect of Triclosan depends on the hepatocyte Est, we pretreated $Est^{\Delta HC}$ mice with Triclosan before ConA injection. The serum ALT and AST levels and liver necrosis analysis showed that the ConA-treated $Est^{\Delta HC}$ mice were no longer protected by Triclosan (Fig. S3, *A*–*C*), suggesting that the protection was hepatocyte Est dependent. Interestingly, we did not observe an increased expression of c-IAP1 and c-IAP2 in ConA-treated $Est^{\Delta HC}$ mice (Fig. S3*D*), suggesting that loss of Est in other cell types may

staining of liver sections. The scale bars represent 100 μm. *Dashed lines* and "*N*" indicate necrosis. *E* and *F*, Western blotting (*E*) and its quantification (*F*) of Bax in liver samples collected from WT and EstKO mice treated with ConA for 6 h. *G* and *H*, hepatic mononuclear cells harvested at 6 h after ConA administration were analyzed by flow cytometry. n = 3 per group. Data are presented as mean ± SD; $^*p < 0.05$, $^{**}p < 0.01$, $^{***}p < 0.001$, $^{****}p < 0.0001$.

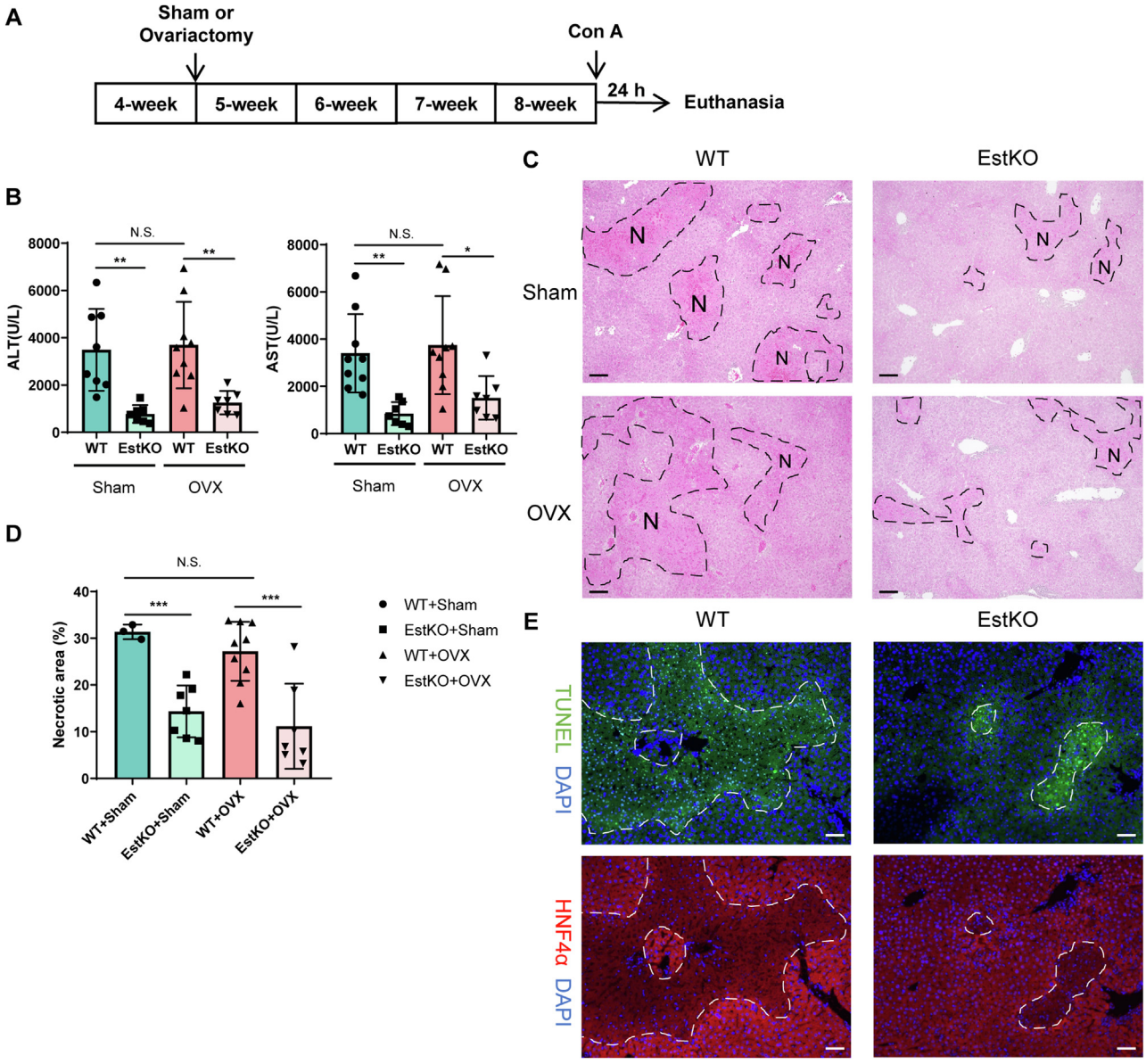

Figure 4. The attenuation of ConA-induced hepatitis in female EstKO mice is independent of estrogens. *A*, four-week-old WT and EstKO female mice were subjected to ovariectomy (OVX), and ConA was injected 4 weeks after the surgery. *B*, serum ALT and AST levels. *C*, liver histology by H&E staining. *D*, quantification of necrotic area in liver histology. *E*, immunofluorescence staining of HNF4α and TUNEL staining of liver sections. The scale bars represent 100 μm. *Dashed lines* and "*N*" indicate necrosis. n = 7 to 9 per group as shown in plots. Data are presented as mean ± SD; N.S., statistically not significant, $^{*}p < 0.05$, $^{**}p < 0.01$, $^{***}p < 0.001$, the comparisons are indicated. ALT, alanine aminotransferase; AST, aspartate aminotransferase; TUNEL, terminal deoxynucleotidyl transferase dUTP nick end labeling.

have also contributed to the regulation of c-IAP1 and c-IAP2 in EstKO mice.

Lcn2 is upregulated in EstKO mice, and loss of Lcn2 abolishes the protective phenotype of Est ablation

To investigate the mechanism by which Est ablation protected mice from ConA-induced AIH, we performed RNA sequencing (RNA-Seq) analysis on the livers of ConA-treated WT and EstKO mice. Differential gene expression analysis showed that the expression of lipocalin-2 (Lcn2) was upregulated in the liver of EstKO mice (Fig. 7*A*). Lcn2, an important molecule in innate immunity, has been reported to be inducible by and play a protective role in acute liver injuries, such as those induced by ConA, CCl_4, lipopolysaccharide, and bile duct ligation, because $Lcn2^{-/-}$ mice were more sensitive to these acute liver injuries (15). The upregulation of hepatic Lcn2 in EstKO mice was verified at the mRNA level by real-time PCR (Fig. 7*B*) and at the protein level by both Western blotting (Fig. 7*C*) and immunohistochemistry staining (Fig. 7*D*). The upregulation of Lcn2 was abolished in KOLE mice at both the mRNA and protein levels (Fig. 7, *B–D*), suggesting that the induction of Lcn2 may have contributed to the protective phenotype of EstKO mice. To test this hypothesis, we created Est and Lcn2 double-knockout (DKO) mice by crossbreeding EstKO mice with Lcn2KO mice. Lcn2KO mice were more sensitive to ConA-induced liver

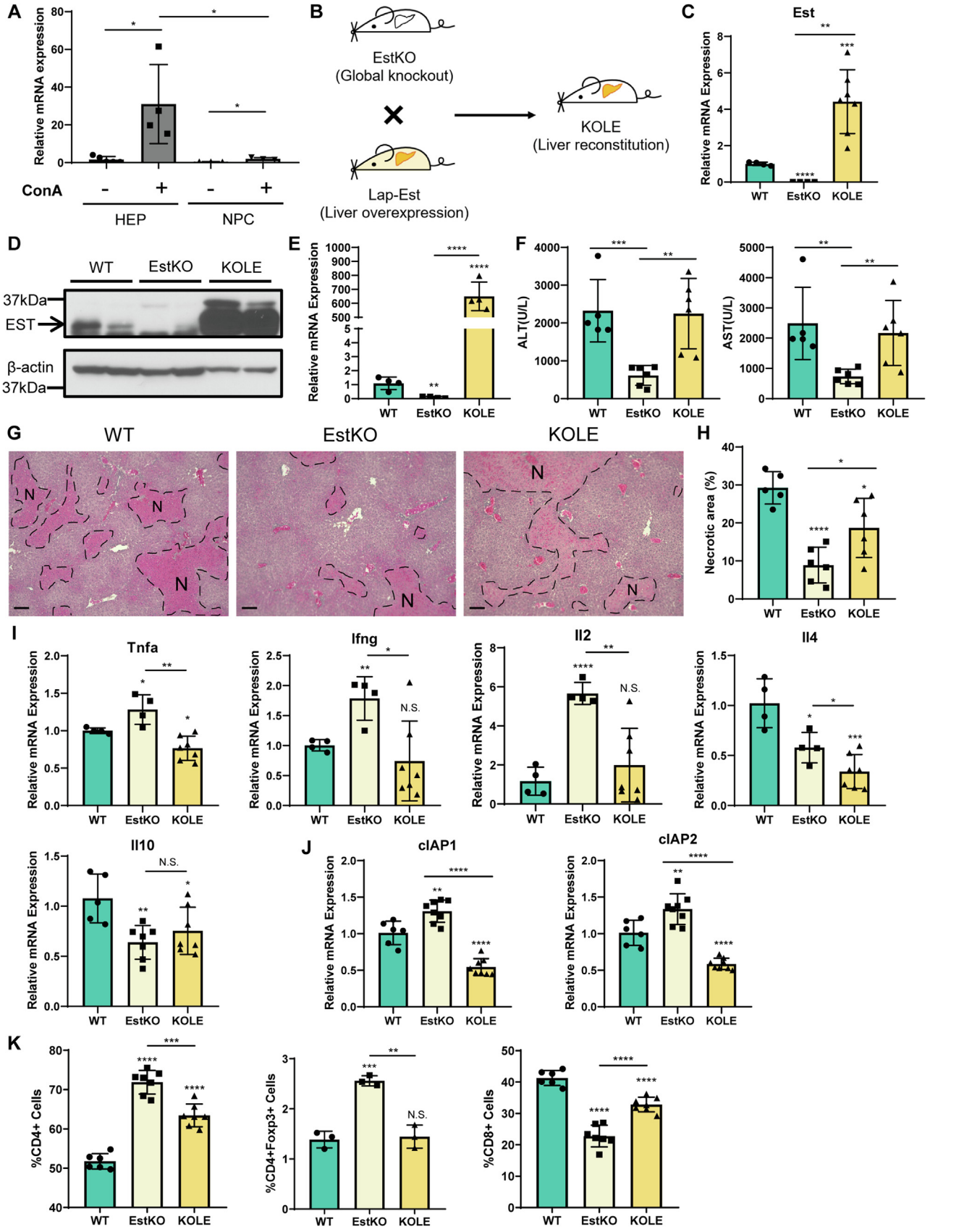

Figure 5. Hepatocyte-specific reconstitution of Est abolishes the ConA protective phenotype of EstKO mice. *A*, mRNA expression of Est in hepatocytes (HEP) and nonparenchymal cells (NPC) isolated from mice treated with or without ConA. n = 3 to 5 per group as shown in plots. *B*, schematic representation of reconstitution of Est in the hepatocytes of EstKO mice by the creation of KOLE mice. *C*, mRNA expression of Est in the liver tissue. *D* and *E*, protein (*D*) and mRNA (*E*) expression of Est in primary hepatocytes. *F–H*, eight-week-old WT, EstKO, and KOLE female mice were treated with 10 mg/kg ConA by tail vein

injury than the WT mice as shown by the serum AST level (Fig. 7*E*) and liver necrosis (Fig. 7, *F* and *G*), consistent with a previous report (15). In the Lcn2KO background, Est ablation no longer protected mice from ConA-induced hepatitis, as shown by the serum ALT and AST levels (Fig. 7*E*) and liver necrosis (Fig. 7, *F* and *G*). Moreover, the expressions of cytokines, including Tnfα, Ifnγ, Il2, Il4, and Il10, were no longer different between Lcn2KO mice and DKO mice (Fig. 7*H*). When the immune cell infiltrations were evaluated and compared with the Lcn2KO mice, the percentages of Tregs and $CD8^+$ T cells remained unchanged, but the total $CD4^+$ T cells were still increased in the DKO mice (Figs. 7*I* and S4). These results suggested that the expression and regulation of Lcn2 were required for the protective effect of Est ablation on ConA-induced hepatitis.

Discussion

AIH remains a major health concern due to its severity and the lack of specific therapeutic strategies. Treatment with glucocorticoids is the mainstay, but not all patients are responsive to glucocorticoids and over 80% of responsive patients may develop late relapses (2). Thus, it is urgent to better understand the pathophysiology of AIH with the hope to identify novel therapeutic targets and design better and more specific therapies.

Our most interesting finding is defining Est as the key cellular factor for the female predisposition to AIH. The female preponderance of AIH is well known in the clinic, which has been recapitulated in the ConA model ((7) and our data not shown). However, the molecular basis for the female preponderance has been elusive. In this study, we showed genetic ablation or pharmacological inhibition of Est protected female mice from ConA-induced hepatitis, suggesting that Est is required for the female sensitivity to AIH. Interestingly, we found that the protective effect of Est inhibition was estrogen independent. This was a surprise, considering that the primary female sex hormone estrogen is the best-known substrate of Est and sulfonated estrogens are no longer hormonally active. The ablation and inhibition of Est can lead to an accumulation of estrogens due to the compromised estrogen deactivation, which has been proposed to be the mechanism for the protective phenotype of Est ablation in liver ischemia and reperfusion (10), sepsis (11), and hemorrhagic shock-induced acute lung injury (13). Knowing estrogens can attenuate immune responses (19), we initially hypothesized that the protective phenotype of EstKO mice might be dependent on estrogens. To our surprise, the ovariectomized EstKO mice and $Est^{\Delta HC}$ mice remained protected from ConA-induced AIH, suggesting that the protection was unlikely mediated by the accumulation of estrogens. The estrogen-independent protective effect of Est ablation was also reported in the acute kidney injury model (12). Interestingly, the male EstKO mice were not protected from ConA-induced liver injury (data not shown), suggesting that, although estrogens did not appear to play a role in the protective phenotype of female EstKO mice, the effect of Est ablation on T cell–mediated hepatitis was sex specific, but the mechanism for the sexual dimorphism remains to be understood. Nevertheless, it remains to be determined whether the protective effect of Est ablation on AIH is due to Est substates other than the estrogens or Est has biological functions other than its sulfotransferase activity.

Given the anti-inflammatory activity of estrogens, another surprising finding is that the protective phenotype of Est ablation was accompanied by the induction of proinflammatory cytokines Tnfα and Ifnγ. This result was counterintuitive, because the induction of Tnfα and Ifnγ has been proposed to be responsible for the sensitizing effect of liver X receptor α (LXRα) activation in the ConA model (20). The inflammatory response is a double-edged sword and in the case of TNFα and upon binding to its receptor, TNFα can either induce apoptosis or activate NF-κB and MAPK signaling facilitated by the prosurvival proteins c-IAP1 and c-IAP2 (18). In our ConA-treated EstKO mice, the expression levels of c-IAP1 and c-IAP2 were elevated, whereas apoptosis was suppressed, providing a plausible mechanism by which Est ablation protected mice from ConA-induced AIH. However, the mechanism by which Est ablation enhances the ConA-responsive induction of Tnfα and Ifnγ and leads to an overall survival response remains to be fully understood.

In addition to the induction of Tnfα and Ifnγ, the Est ablation responsive induction of Lcn2 may have also contributed to the protective phenotype. The induction of Lcn2 in EstKO mice was first suggested by our RNA-Seq analysis. We went on to show that the induction of Lcn2 was functionally relevant, because concurrent ablation of Lcn2 abolished the protective phenotype of Est ablation. Interestingly, the sensitization of Lcn2KO mice to ConA was reported to be associated with an increased hepatic expression of inflammatory cytokines Tnfα, Ifnγ, Il6, Il1a, Il1b, Il2, and Il10 (15). However, in our study, the expression of Ifnγ, Il4, Il2, and Il10 was modestly but significantly decreased, while the expression of Tnfα remains unchanged in ConA-treated Lcn2KO mice. The mechanism for these discrepancies remains to be understood, but our most notable observation was that the upregulation of Tnfα and Ifnγ in ConA-treated EstKO mice was abolished in DKO mice, further suggesting the induction of these proinflammatory cytokines played a role in the protective phenotype of EstKO mice. The mechanism by which Est ablation induces Lcn2 remains to be understood. Also, Lcn2 is expressed in many tissues including the liver, and within the liver, Lcn2 is expressed in multiple hepatic cell types. The use of whole

injections, and the tissues and serum were collected at 24 h after ConA administration. n = 5 to 6 per group as shown in plots. *F*, serum ALT and AST levels. *G*, liver histology by H&E staining. *Dashed lines* and "*N*" indicate necrosis. The scale bars represent 100 μm. *H*, quantification of necrotic area in liver histology. *I*, the mRNA expression of inflammatory cytokines in the liver tissues. *J*, the mRNA expression of prosurvival protein genes c-IAP1 and c-IAP2 in the liver tissues. *K*, hepatic mononuclear cells harvested at 6 h after ConA challenge were analyzed by flow cytometry. Shown are percentages of $CD4^+$, $CD4^+Foxp3^+$, $CD8^+$ cells. n = 3 to 7 per group as shown in plots. Data are presented as mean ± SD; N.S., statistically not significant, $^*p < 0.05$, $^{**}p < 0.01$, $^{***}p < 0.001$, $^{****}p < 0.0001$, compared with WT control or the comparisons are labeled.

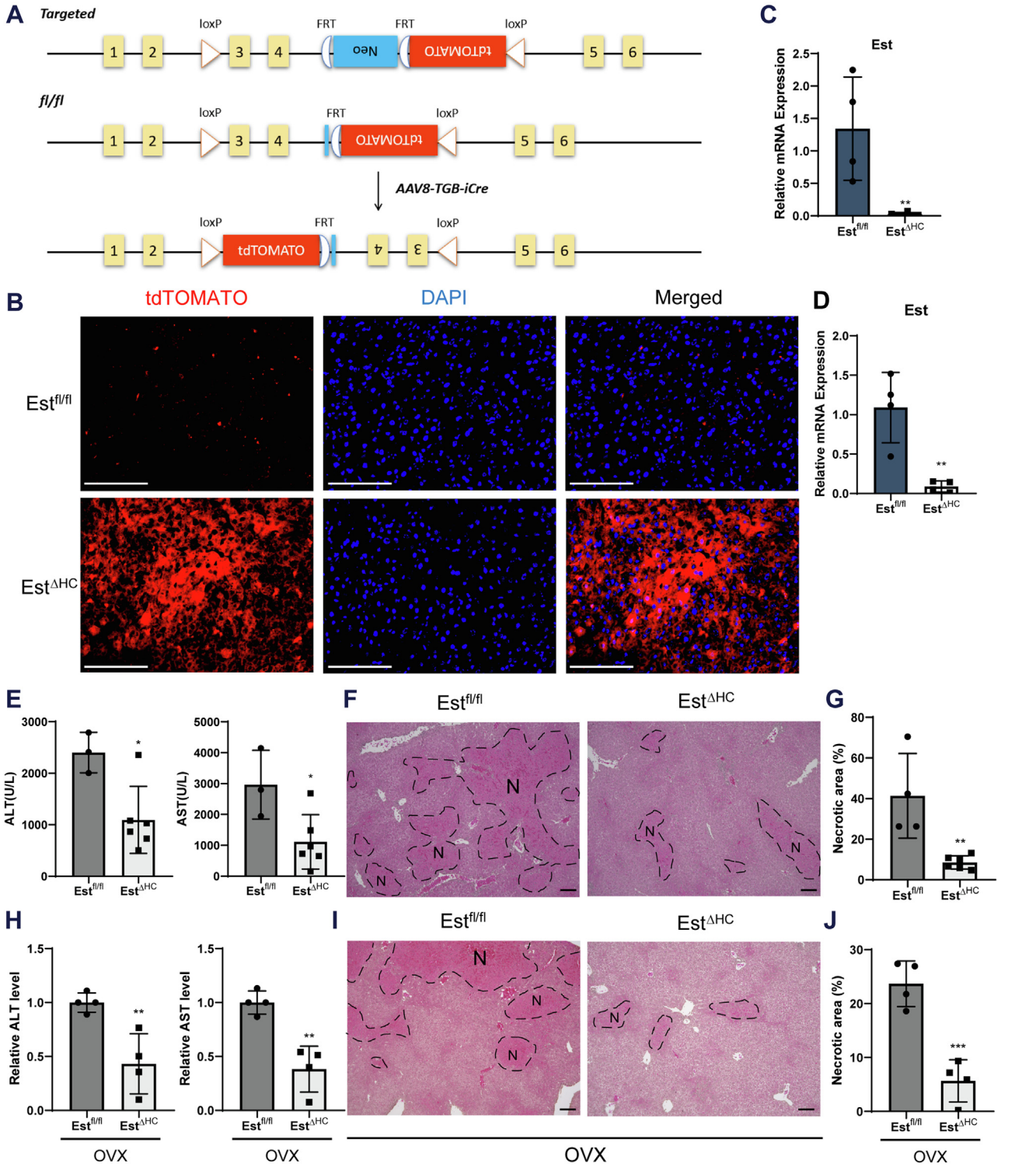

Figure 6. Hepatocyte-specific ablation of Est protects mice from ConA-induced hepatitis independent of estrogens. *A*, schematic representation of the creation of the conditional $Est^{fl/fl}$ mice and the outcome of Est knockout upon the AAV8-TBG-iCre infection. *B*, fluorescence signals of tdTOMATO and DAPI in the liver cryosections. The scale bars represent 100 μm. *C*, mRNA expression of Est in the liver tissue. *D*, mRNA expression of Est in primary hepatocytes. *E–G*, six-week-old $Est^{fl/fl}$ female mice were infected with AAV8-TBG-eGFP or AAV8-TBG-iCre by tail vein injection, and ConA was administered 2 weeks after the viral infections. Tissues and serum were collected at 24 h after ConA administration. n = 3 to 6 per group as shown in plots. *H–J*, four-week-old $Est^{fl/fl}$ female mice were subjected to ovariectomy (OVX). Ovariectomized mice were infected with AAV8-TBG-eGFP or AAV8-TBG-iCre 2 weeks after the surgery, and ConA was administered 2 weeks after the viral infections. Tissues and serum were collected at 24 h after ConA administration. n = 4 per group. Shown are serum ALT and AST levels (*E* and *H*), liver histology by H&E staining (*F* and *I*), and quantification of necrotic area in liver histology (*G* and *J*). *Dashed lines* and "*N*" indicate necrosis. The scale bars represent 100 μm. Data are presented as mean ± SD; $*p < 0.05$, $**p < 0.01$, $***p < 0.001$. ALT, alanine aminotransferase; AST, aspartate aminotransferase.

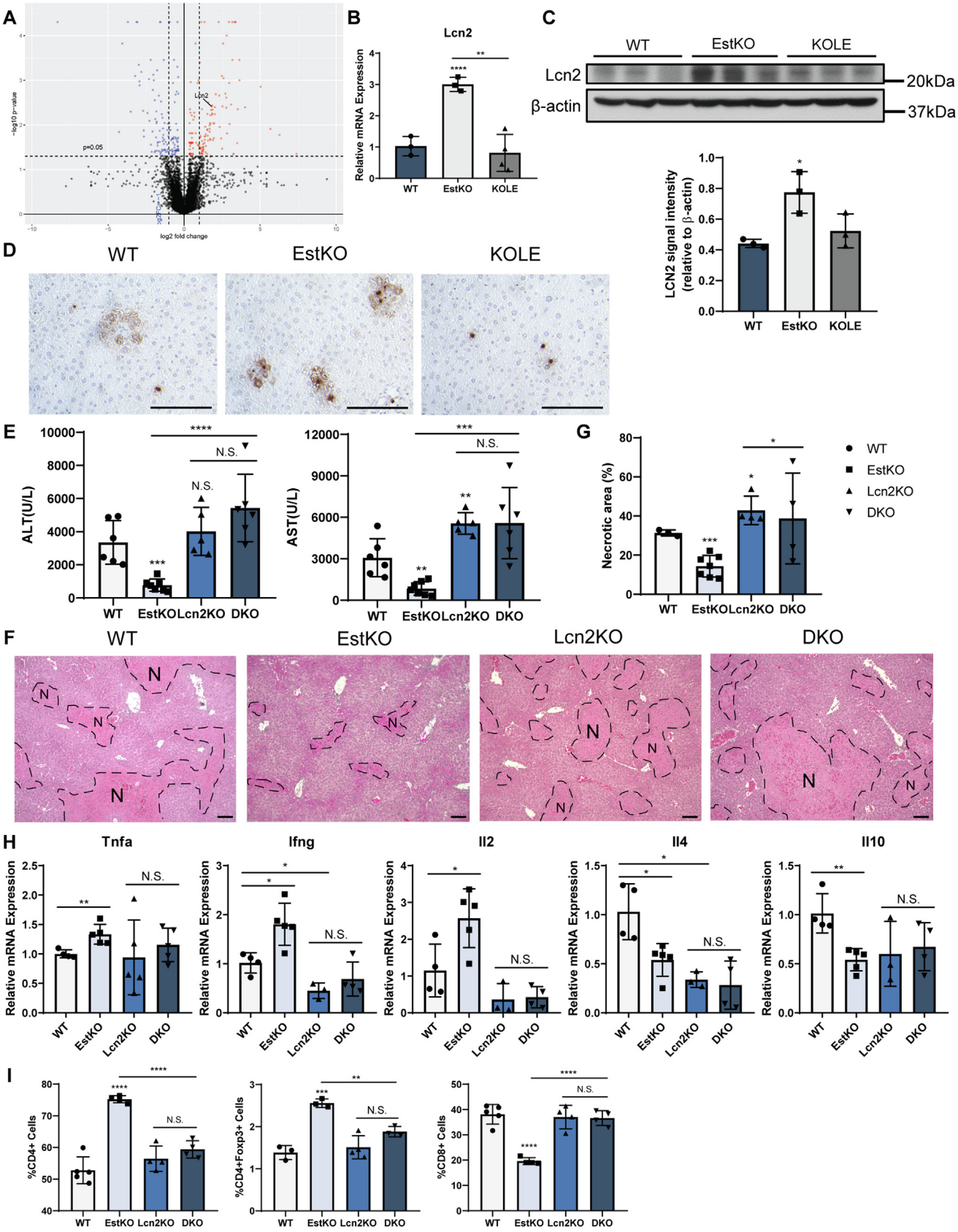

Figure 7. Lcn2 is upregulated in EstKO mice, and loss of Lcn2 abolishes the protective phenotype of Est ablation. *A*, volcano plot of differentially expressed genes (EstKO *versus* WT) in liver tissue analyzed by RNA sequencing. *B*, expression of Lcn2 in the liver tissue measured by quantitative PCR. *C*, protein expression of Lcn2 in liver tissue measured by Western blotting and its quantification shown in the bar graph below. *D*, immunohistochemistry staining of Lcn2 in liver paraffin sections. The scale bars represent 100 μm. *E–H*, eight-week-old WT, EstKO, Lcn2KO, and DKO female mice were treated with

body Lcn2KO mice prevented us from pinpointing the cellular source of Lcn2 that contributed to the phenotype.

Another interesting finding of this study is the tissue- and cell type–specific effect of Est on ConA-induced AIH. Est is expressed in multiple tissues and multiple cell types within the same tissue. Upon the ConA challenge, the induction of Est was dramatic in the hepatocytes but negligible in NPCs. Conditional ablation of Est in the hepatocytes phenocopied the protection observed in ConA-treated global EstKO mice. In our gain-of-function model, transgenic reconstitution of Est in the hepatocytes abolished the protective phenotype of EstKO mice, further supporting that loss of Est in the hepatocytes was responsible for the protection. The tissue-specific effect of Est was also reported in our previous characterization of the Est-deficient ob/ob mice, in which the reconstitution of Est in the adipose tissues but not in the liver improved the metabolic functions of the Est-deficient ob/ob mice (9). In another example, reconstitution of Est in the liver abolished the renoprotective phenotype of EstKO mice in the acute kidney injury model (12).

In summary, we have unveiled a novel function of hepatic Est in ConA-induced AIH. The hepatic expression of Est is required for the female sensitivity to ConA-induced hepatitis independent of estrogens. Our results suggest that pharmacological inhibition of Est, at least in females, may represent a novel therapeutic strategy for the clinical management of AIH and other T cell–mediated hepatitis.

Experimental procedures

Mice

Female wildtype (WT), Est knockout (EstKO), KOLE, $Est^{fl/fl}$, Lcn2 knockout (Lcn2KO), and Est and Lcn2 double knockout (DKO) mice in the C57BL/6 background, 8 to 10 weeks old, were used. WT and Lcn2KO mice were obtained from the Jackson Laboratory and cohoused with the other mouse groups. The whole-body EstKO mice have been described (21). KOLE mice were generated by crossbreeding the EstKO mice with the liver-specific EST transgenic (LE) mice as described (12). $Est^{fl/fl}$ mice with the third and fourth exons of the mouse Est gene floxed were custom generated by the Ingenious Targeting Laboratory. The hepatocyte-specific knockout of Est was achieved by infecting the $Est^{fl/fl}$ mice with AAV8-TBG-eGFP or AAV8-TBG-iCre purchased from Vector Biolabs at the dose of 1×10^{11} genome copies per mouse by tail vein injection 2 weeks before subjecting the mice to the ConA model of AIH. DKO mice were generated by crossbreeding EstKO mice and Lcn2KO mice. Ovariectomy surgery was performed at 4 weeks of age. Ovaries were removed after a small abdominal incision. Sham-operated mice underwent the same procedure as the ovariectomized mice but without resection of the ovaries. Mice were housed *ad libitum* on a 12-h/12-h light/dark cycle under pathogen-free conditions. All experimental procedures were performed in accordance with relevant federal guidelines and with the approval of the University of Pittsburgh Institutional Animal Care and Use Committee.

Concanavalin A model of AIH

Concanavalin A (ConA) purchased from Alfa Aesar was dissolved in saline and administrated by tail vein injections at the dose of 10 mg/kg for all experiments. When necessary, Triclosan purchased from Sigma-Aldrich was administered by s.c. injections daily at the dose of 20 mg/kg beginning 2 days before the ConA treatment and until the day of ConA injection. Mice were sacrificed at indicated time points after the ConA injection for serum and liver tissue harvest. Blood was collected *via* cardiac puncture and subsequently centrifuged twice at 8000*g* for 5 min to collect the serum. Liver tissues were fixed in 10% formalin for histology or snap-frozen on dry ice and stored at −80 °C until further analysis.

Serum biochemistry and cytokine measurements

The serum levels of ALT and AST were measured by using enzymatic assay kits from Stanbio Laboratory. The serum levels of TNFα and IFNγ were measured by ELISA kits from R&D Systems.

Liver histology, immunohistochemistry, immunofluorescence, and fluorescence imaging

Liver tissues were fixed in 10% neutral buffered formalin for 24 h, and then dehydrated, embedded in paraffin, sectioned at 4 μm, and processed for hematoxylin and eosin (H&E) staining. The areas of hepatic necrosis were quantified using the NIH ImageJ software by examining ten random fields at 10× magnification and expressed as a percentage of necrotic area per total area examined. For immunohistochemistry and immunofluorescence staining of Est, Lcn2, and HNF4α, antigen retrieval was performed by heat-mediated epitope retrieval in citric acid solution for 20 min. The primary antibodies of Est, Lcn2, and HNF4α and the secondary antibody of HNF4α immunofluorescence are listed in Table S1 The VECTASTAIN ABC Kit (PK-6101) was used, and the staining was visualized using the DAB Peroxidase Substrate Kit (SK-4105) from Vector Laboratories. TUNEL staining was performed by using the *In Situ* Cell Death Detection Kit from Roche. For tdTOMATO imaging, liver tissues were fixed in 1% paraformaldehyde PBS at 4 °C for 4 h and placed in 30% sucrose at 4 °C overnight. Specimens then were frozen in Tissue-plus O.C.T, sectioned, and mounted with DAPI Fluoromount-G. Images of TUNEL staining, tdTOMATO/Cy3, and DAPI

10 mg/kg ConA by tail vein injections, and the tissues and serum were collected at 24 h after ConA administration. n = 4 to 7 per group as shown in plots. Shown are serum ALT and AST levels (*E*); liver histology by H&E staining (*F*) (the representative images of ConA-treated WT and EstKO mice are reused from Fig. 2*B* since they are the same groups of mice), *dashed lines* and "*N*" indicate necrosis, the scale bars represent 100 μm; quantification of necrotic area in liver histology (*G*); and the mRNA expression of inflammatory cytokines in liver tissues (*H*). *I*, hepatic mononuclear cells harvested at 6 h after ConA challenge were analyzed by flow cytometry. Shown are percentages of $CD4^+$, $CD4^+Foxp3^+$, $CD8^+$ cells. n = 4 to 7 per group as shown in plots. Data are presented as mean ± SD; N.S., statistically not significant, $^*p < 0.05$, $^{**}p < 0.01$, $^{***}p < 0.001$, $^{****}p < 0.0001$, compared with WT control or the comparisons are labeled. ALT, alanine aminotransferase; AST, aspartate aminotransferase.

were acquired using the fluorescence microscope (BZ-X810) from KEYENCE by using the GFP, TRITC, and DAPI filters, respectively.

Primary hepatocytes and nonparenchymal cells isolation

Primary liver cells were isolated by a combination of collagenase digestion and centrifugal elutriation as described (22, 23). Briefly, the mouse livers were perfused through the superior vena cava by 0.2 mM EGTA and 5 mg/ml Liberase TM. The liver cell suspensions were filtered through a 100-μm cell strainer to eliminate undigested tissue remnants. Hepatocytes were collected from the pellet after centrifugation twice at 500 rpm for 3 min. The supernatant was centrifuged at 300*g* for 10 min. The pellet was resuspended in 35% (vol/vol) Percoll Plus solution and centrifuged at 500*g* for 15 min. NPCs were collected from the pellet, which was suspended in ACK Lysing Buffer from BD Biosciences and washed.

Flow cytometry analysis

Hepatic MNCs and splenic lymphocytes were isolated as described (20). The cells were first stained for surface markers with their antibodies 1:200 diluted in fluorescence-activated cell sorting buffer, fixed, and permeabilized with Intracellular Fixation & Permeabilization Buffer from eBioscience, and then subjected to the intracellular Foxp3 staining. The conjugated antibodies used for flow cytometric analysis are listed in Table S1 After staining, cells were washed with the fluorescence-activated cell sorting buffer and analyzed on LSRFortessa at the University of Pittsburgh Flow Cytometry Core Facility. The flow cytometry data were analyzed with the FlowJo software from Treestar. The gating strategies are shown in Fig. S1.

Real-time quantitative PCR and Western blot analysis

Total tissue RNA was extracted with TRIzol reagent from Invitrogen. Complementary DNA (cDNA) was synthesized, and SYBR Green based real-time PCR was performed using the QuantStudio 6 Flex Real-Time PCR System. Data were normalized to the control cyclophilin by the ΔΔCt method. PCR primer sequences are listed in Table S2 For Western blot analysis, 30 μg of protein extracts was separated on SDS-PAGE gels and transferred onto a polyvinylidene difluoride (PVDF) membrane. The primary antibodies of Est, Lcn2, and Bax are listed in Table S1.

RNA sequencing analysis

Total RNA was extracted with the RNeasy Mini Kit and subjected to library preparation. RNA-Seq was performed by the Health Sciences Sequencing Core at the Children's Hospital of Pittsburgh. RNA-Seq analysis was performed as we have described (24).

Statistical analysis

Statistical analyses were performed using GraphPad Prism software from GraphPad. Values for all measurements are presented as mean ± standard deviation of the mean. Statistical analyses were performed using the two-tailed Student's *t* test. *p* Values of less than 0.05 were considered statistically significant.

Data availability

The data described in the article are included in the main file and supporting information. Derived data supporting the findings of this study are available from the corresponding author W. X. upon request.

Supporting information—This article contains supporting information.

Author contributions—J. W. and W. X. conceptualization; J. W. and W. X. methodology; Z. Z., J. G., H.-C. T., J. X., H. H., and Y. C. validation; J. W., Z. Z., J. G., H.-C. T., J. X., H. H., Y. C., S. L., M. Z., and D. Y. formal analysis; J. W., Z. Z., J. G., H.-C. T., J. X., H. H., and Y. C. investigation; M. X. and S. R. resources; J. W. data curation; J. W. writing – original draft; W. X. writing – review & editing; J. W., S. L., M. Z., and D. Y. visualization; S. L., M. Z., D. Y., and W. X. supervision; J. W. project administration; W. X. funding acquisition.

Funding and additional information—This work was supported in part by the National Institutes of Health grant ES030429 (to W. X.). The content is solely the responsibility of the authors and does not necessarily represent the official views of the National Institutes of Health.

Conflict of interest—The authors declare that they have no conflicts of interest with the contents of this article.

Abbreviations—The abbreviations used are: AAV8, adeno-associated virus vector serotype 8; AIH, autoimmune hepatitis; ALT, alanine aminotransferase; AST, aspartate aminotransferase; ConA, concanavalin A; DKO, double knockout; Est, estrogen sulfotransferase; IFNγ, interferon gamma; IL-2, interleukin 2; IL-4, interleukin 4; IL-10, interleukin 10; Lcn2, lipocalin2; MNC, mononuclear cells; NPC, nonparenchymal cell; TBG, thyroxine-binding globulin; TNFα, tumor necrosis factor alpha; Treg, regulatory T cell; TUNEL, terminal deoxynucleotidyl transferase dUTP nick end labeling.

References

1. Webb, G. J., Hirschfield, G. M., Krawitt, E. L., and Gershwin, M. E. (2018) Cellular and molecular mechanisms of autoimmune hepatitis. *Annu. Rev. Pathol.* **13**, 247–292
2. Mieli-Vergani, G., Vergani, D., Czaja, A. J., Manns, M. P., Krawitt, E. L., Vierling, J. M., *et al.* (2018) Autoimmune hepatitis. Nat. Rev. Dis. Primers **4**, 18017
3. Liberal, R., Grant, C. R., Mieli-Vergani, G., and Vergani, D. (2013) Autoimmune hepatitis: a comprehensive review. *J. Autoimmun.* **41**, 126–139
4. Heymann, F., Hamesch, K., Weiskirchen, R., and Tacke, F. (2015) The concanavalin a model of acute hepatitis in mice. *Lab. Anim.* **49**, 12–20
5. Wang, H. X., Liu, M., Weng, S. Y., Li, J. J., Xie, C., He, H. L., *et al.* (2012) Immune mechanisms of concanavalin a model of autoimmune hepatitis. World J. Gastroenterol. **18**, 119–125

6. Ballegeer, M., and Libert, C. (2016) Different cell types involved in mediating concanavalin a induced liver injury: a comprehensive overview. *J. Gastroenterol. Hepatol. Res.* **1**, 1–13
7. Takamoto, S., Nakamura, K., Yoneda, M., and Makino, I. (2003) Gender-related differences in concanavalin A-induced liver injury and cytokine production in mice. *Hepatol. Res.* **27**, 221–229
8. Barbosa, A. C. S., Feng, Y., Yu, C., Huang, M., and Xie, W. (2019) Estrogen sulfotransferase in the metabolism of estrogenic drugs and in the pathogenesis of diseases. *Expert Opin. Drug Metab. Toxicol.* **15**, 329–339
9. Gao, J., He, J., Shi, X., Stefanovic-Racic, M., Xu, M., O'Doherty, R. M., *et al.* (2012) Sex-specific effect of estrogen sulfotransferase on mouse models of type 2 diabetes. Diabetes **61**, 1543–1551
10. Guo, Y., Hu, B., Huang, H., Tsung, A., Gaikwad, N. W., Xu, M., *et al.* (2015) Estrogen sulfotransferase is an oxidative stress-responsive gene that gender-specifically affects liver ischemia/reperfusion injury. *J. Biol. Chem.* **290**, 14754–14764
11. Chai, X., Guo, Y., Jiang, M., Hu, B., Li, Z., Fan, J., *et al.* (2015) Oestrogen sulfotransferase ablation sensitizes mice to sepsis. *Nat. Commun.* **6**, 7979
12. Silva Barbosa, A. C., Zhou, D., Xie, Y., Choi, Y. J., Tung, H. C., Chen, X., *et al.* (2020) Inhibition of estrogen sulfotransferase (SULT1E1/EST) ameliorates ischemic acute kidney injury in mice. *J. Am. Soc. Nephrol.* **31**, 1496–1508
13. Xie, Y., Barbosa, A. C. S., Xu, M., Oberly, P. J., Ren, S., Gibbs, R. B., *et al.* (2020) Hepatic estrogen sulfotransferase distantly sensitizes mice to hemorrhagic shock-induced acute lung injury. *Endocrinology* **161**, bqz031
14. Asimakopoulou, A., Weiskirchen, S., and Weiskirchen, R. (2016) Lipocalin 2 (LCN2) expression in hepatic malfunction and therapy. *Front. Physiol.* **7**, 430
15. Borkham-Kamphorst, E., van de Leur, E., Zimmermann, H. W., Karlmark, K. R., Tihaa, L., Haas, U., *et al.* (2013) Protective effects of lipocalin-2 (LCN2) in acute liver injury suggest a novel function in liver homeostasis. *Biochim. Biophys. Acta* **1832**, 660–673
16. Rani, R., Tandon, A., Wang, J., Kumar, S., and Gandhi, C. R. (2017) Stellate cells Orchestrate concanavalin A-induced acute liver damage. *Am. J. Pathol.* **187**, 2008–2019
17. James, M. O., Li, W., Summerlot, D. P., Rowland-Faux, L., and Wood, C. E. (2010) Triclosan is a potent inhibitor of estradiol and estrone sulfonation in sheep placenta. *Environ. Int.* **36**, 942–949
18. Webster, J. D., and Vucic, D. (2020) The balance of TNF mediated pathways regulates inflammatory cell death signaling in healthy and diseased tissues. *Front. Cell Dev. Biol.* **8**, 365
19. Straub, R. H. (2007) The complex role of estrogens in inflammation. *Endocr. Rev.* **28**, 521–574
20. Gao, L., Li, B., Wang, J., Shen, D., Yang, M., Sun, R., *et al.* (2020) Activation of liver X receptor alpha sensitizes mice to T-cell mediated hepatitis. *Hepatol. Commun.* **4**, 1664–1679
21. Qian, Y. M., Sun, X. J., Tong, M. H., Li, X. P., Richa, J., and Song, W. C. (2001) Targeted disruption of the mouse estrogen sulfotransferase gene reveals a role of estrogen metabolism in intracrine and paracrine estrogen regulation. *Endocrinology* **142**, 5342–5350
22. Aparicio-Vergara, M., Tencerova, M., Morgantini, C., Barreby, E., and Aouadi, M. (2017) Isolation of kupffer cells and hepatocytes from a single mouse liver. *Methods Mol. Biol.* **1639**, 161–171
23. Li, H., Feng, D., Cai, Y., Liu, Y., Xu, M., Xiang, X., *et al.* (2018) Hepatocytes and neutrophils cooperatively suppress bacterial infection by differentially regulating lipocalin-2 and neutrophil extracellular traps. *Hepatology* **68**, 1604–1620
24. Wang, Z., Yang, B., Zhang, M., Guo, W., Wu, Z., Wang, Y., *et al.* (2018) lncRNA epigenetic landscape analysis identifies EPIC1 as an oncogenic lncRNA that interacts with MYC and promotes cell-cycle progression in cancer. *Cancer Cell* **33**, 706–720.e9